Available online at www.sciencedirect.com
SCIENCE DIRECT®
Remote Sensing of Environment 90 (2004) 405–414
Remote Sensing of Environment
www.elsevier.com/locate/rse

NASA EOS Terra ASTER: Volcanic topographic mapping and capability

Nicki F. Stevens[a,*], Harold Garbeil[b], Peter J. Mouginis-Mark[b]

[a] Department of Natural Hazards Group, Institute of Geological and Nuclear Sciences, 69 Gracefield Road 6315, Lower Hutt, Wellington, New Zealand
[b] Hawaii Institute of Geophysics and Planetology, University of Hawaii, 1680 East-West Road, Honolulu, HI 96822, USA

Received 8 November 2003; received in revised form 13 January 2004; accepted 22 January 2004

Abstract

Up-to-date, accurate topographic data are a crucial resource for volcanic research and risk mitigation efforts, in particular, for modeling volcanic flow processes at a detailed spatial resolution. In this paper, we examine the utility of the Advanced Spaceborne Thermal Emission and Reflection Radiometer (ASTER) instrument currently operating on the NASA Terra satellite, which provides near infrared (VNIR) stereo imaging from which topography can be derived. We wrote software to generate digital elevation models (DEMs) from the ASTER level 1A product, which employs an automated stereo matching technique to calculate the parallax offsets between the images acquired by the nadir- and aft-looking sensors. Comparison of ASTER DEMs with DEMs derived from other sources (digitized 1:50 K topographic maps and aerial interferometric radar) at Ruapehu volcano reveal an RMS error of about 10 m for the ASTER DEM, in the absence of significant atmospheric water vapor. A qualitative assessment of surface features showed that the ASTER DEM is superior to the interpolated 1:50 K map product but falls short of the detail provided by aerial interferometric radar, especially in terms of stream channel preservation. A second ASTER DEM was generated for Taranaki volcano, where previously only 1:50 K topographic map data were available. Although the 2000 Space Shuttle radar topography mission (SRTM) will largely remedy the previous global paucity of adequate topographic data at volcanoes, such as Taranaki, we anticipate the problem that at active volcanoes, the topography may change significantly following activity, rendering the SRTM data inaccurate. With the high temporal coverage of the dataset, ASTER not only provides a means to update significant (>10 m) topographic measurements at active volcanoes via a time-series of DEMs, but also provides a simultaneous means to map surface cover and localized land-use via the near infrared sensors. Thus we demonstrate the potential for up-to-date volcanic economic risk assessment using geographic information systems (GIS) analysis.

Keywords: EOS Terra ASTER; Digital elevation model (DEM); Vertical accuracy; Surface feature preservation; Taranaki/Egmont; Ruapehu; Applications

1. Introduction

A large proportion of volcanic research and risk mitigation is underpinned by the availability of reliable topographic data. For example, state-of-the-art methods to delineate areas at risk at active volcanoes include the use of computer models that simulate the path of volcanic flows over digital representations of the local topography, or digital elevation models (DEMs) (e.g. Ishihara et al., 1990; Schilling, 1998). The reliability of such studies are aided or hindered by the resolution and quality of the DEM available (Stevens et al., 2002), and also on whether the data are up-to-date, a particular concern at active volcanoes, where significant terrain alteration accompanies many eruptions.

Taranaki (also known as Mount Egmont), an active stratovolcano located on the North Island of New Zealand, is a case in point (Fig. 1). Its eruptive history shows that it represents a real future risk to the infrastructure that has been built on its flanks (e.g. Palmer et al., 1991). Obviously, risk delineation by flow modeling would be of benefit here. However, we have shown previously that the errors in DEMs can limit the plausibility of computer models delineating volcanic risk, in terms of updating topographic change and in terms of data quality (Stevens et al., 2002). Prior to this study, the available topographic data covering the Taranaki area were not adequately detailed for this purpose.

The ASTER sensor on the NASA Terra satellite is a high-resolution instrument that provides a near-infrared stereo imaging capability with a spatial resolution of 15 m, and a swath width of 60 km (Abrams, 2000). TERRA has a 16-day repeat interval, and ASTER has an 8% duty cycle, so at

* Corresponding author. Tel.: +64-4-570-4770; fax: +64-4-570-4600.
E-mail address: n.stevens@gns.cri.nz (N.F. Stevens).

0034-4257/$ - see front matter © 2004 Elsevier Inc. All rights reserved.
doi:10.1016/j.rse.2004.01.012

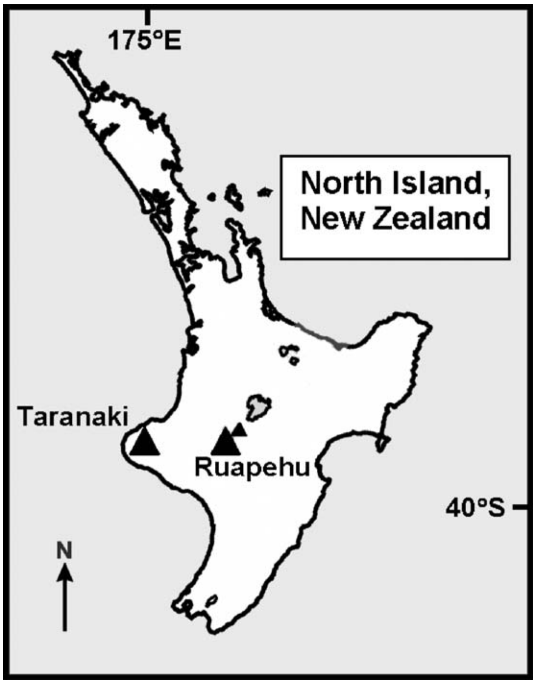

Fig. 1. Map of the North Island of New Zealand, showing locations of Taranaki and Ruapehu volcanoes.

least one or two stereo pairs over any given site are obtained each year, although nominally, the orbital configuration should allow an acquisition approximately every 44 days, scheduling permitting. DEMs produced from ASTER are a standard product provided by the United States Geological Survey (USGS) EROS Data Center (Welch et al., 1998). Understandably, the ordering process, especially for an absolute DEM, is not trivial and the delivery time may be many weeks. To speed up access to the data following major topographic change, when updates are needed as quickly as possible, we have developed our own software and capability to do the automated matching and data processing directly from ASTER stereo images. The quality of the ASTER-derived DEM data is assessed here qualitatively and quantitatively, in particular by comparison with even higher resolution topographic data from an airborne interferometric radar survey of Ruapehu volcano (Fig. 1), which was obtained in 1996 and 2000 during the NASA PACRIM missions (Stevens et al., 2002).

ASTER data are advantageous because the stereo pair is obtained on the same track, and because the necessary information for deriving topography is provided simultaneously with spectral bands suitable for generating up-to-date land cover maps, using standard image classification techniques. This is an important observational capability, especially at active volcanoes where land surface cover is apt to change as often, or more often, than the topography. In New Zealand, 20th century volcanic activity has already caused significant economic loss (Johnston et al., 2000). If a time-series of cloud-free ASTER data could be obtained, it would provide a powerful observational tool before, during and after significant volcanic topographic and surface change. We thus discuss the applications of the data, including a new, efficient and low-cost methodology to calculate potential economic loss in eastern Taranaki due to major debris avalanching, and consider the relative merits of ASTER DEMs versus the recently released Shuttle radar topography mission (SRTM) topographic dataset.

2. Geological background

2.1. Taranaki (Mt. Egmont)

Taranaki volcano is located on the western coast of the North Island of New Zealand (Fig. 1), 180 km above the subducting Pacific plate (Adams & Ware, 1977). It last erupted around 1655 AD (Neall et al., 1986). Taranaki has a steep-sided (typically $\sim 30^\circ$ slope on the upper flanks), reasonably symmetrical conical morphology, and is surrounded by a ring plain of reworked deposits. The summit elevation is 2500 m above sea level. The cone is thought to be less than 10,000 years in age, with magma ranging in composition from basaltic andesite to andesite (Neall et al., 1986). Field investigations show periodic major sector collapse (Palmer & Neall, 1991), as well as a history of debris avalanches, lava and pyroclastic flows, tephra deposition and lahars, occurring at a range of scales (Alloway et al., 1995; Neall & Alloway, 1993; Neall et al., 1986). The region has a population of just under 103,000 (2001 census), distributed in towns and rurally, and the largest events impacted areas tens of kilometers from the summit (Palmer et al., 1991). Agricultural land use predominates, and the area is also a major centre of on-shore and off shore natural gas and oil extraction in New Zealand.

At the time of writing, the only available topographic data set covering the Taranaki area was the 1:50,000 digitized map contours from the national map series (Land Information New Zealand (LINZ), 1999). Although the LINZ 1:50,000 contours have a root mean square (r.m.s.) vertical accuracy of ~ 8 m (LINZ, 2000; Shearer, 1990), the interpolation between 1:50,000 contours to produce a DEM introduces additional significant errors, especially where contours are spaced widely and are sinuous (Robinson, 1994). Barringer and Lilburne (1997) calculate an r.m.s. vertical accuracy of 8 m for DEMs derived from LINZ data, but Shearer (1990) shows that an additional ± 2.89 m error results from producing DEMs from 1:50,000 scale maps. Thus, the vertical accuracy of the LINZ DEM data is likely to be nearer to ~ 10 m r.m.s. Data will also be available in the near future from the Shuttle Radar Topography Mission (SRTM), and these are a vast improvement over the 1:50 K data (Stevens et al., 2002). SRTM data are currently being released outside of the US at a spatial resolution of 90 and ~ 8 m vertical resolution only, although a 30 m spatial resolution is possible (Werner, 2001).

2.2. Ruapehu

Ruapehu is a composite volcano surrounded by a radial ring-plain (e.g. Hackett & Houghton, 1989), which last erupted in 1995–1996 (Bryan & Sherburn, 1999), and is located in the central North Island of New Zealand (Fig. 1). The summit area (elevation 2797 m a.s.l.) supports a number of perennial snowfields and glaciers while the active crater hosts a hot acidic lake (Christenson & Wood, 1993), making the generation of lahars a particular feature of volcanic activity at Ruapehu. Field evidence also shows a history that includes at least one debris avalanche deposit, as well as widespread tephra and lava deposition (Palmer & Neall, 1989).

Ruapehu is covered by two sets of digital topographic data obtained by different mapping and data processing methods, at different levels of accuracy. First, as for Taranaki, a DEM has been derived from the national 1:50,000 map contours (Land Information New Zealand (LINZ), 1987, 1996a,b, 1997, 1998). Second, the topography was mapped in November 1996 and August 2000 by the NASA TOPSAR interferometric synthetic aperture radar system, which was carried onboard a DC-8 aircraft. The latter DEM has a superior accuracy, which we describe later, but is limited in spatial extent, being obtained in 10 km swaths.

3. Data acquisition

The Terra satellite was launched in 1999 as part of the NASA Earth Observation System (EOS) program (Abrams, 2000), and orbits at an altitude of 705 km with a repeat-pass interval of 16 days. The ASTER visible near-infrared (VNIR) instrument on-board Terra provides an along-track stereo imaging capability from nadir- and aft-looking sensors, at a spatial resolution of 15 m in the case of bands 1, 2 and 3N (Table 1). Successive images of the same area on the surface of the Earth are acquired by each sensor along track from their differing viewing angles, generating the stereo effect from which topographic measurements can be derived (Fig. 2).

In this respect, ASTER along-track stereo mapping has an advantage over other orbital imaging techniques, such as SPOT stereogrammetry (Toutin & Cheng, 2002; Zomer et al., 2002), and ERS radar interferometry (e.g. Zebker et al., 1994), both of which rely on repeat, cross-track acquisitions on subsequent orbits to provide stereo pairs. Changes in climatic conditions between data acquisitions can be troublesome, causing decorrelation between image pairs, a suitable orbital geometry may not be available, and co-eruptive surface change between repeat-pass acquisitions is not uncommon in volcanic terrain (e.g. Wadge et al., 2002). In the case of ERS radar interferometry for topographic mapping, the data are particularly sensitive to decorrelation caused by surface vegetation and moisture changes. ASTER image pairs are taken about a minute apart, and surface change between acquisitions is therefore unlikely. Still, clouds and cloud shadows may cause decorrelation between the two acquisitions, which will result in a poor match at those locations affected or nearby. ASTER is also best suited for areas with clear geomorphic and or albedo differences, which aid the stereo-matching algorithm.

Table 1
ASTER NVIR bands

Band	Wavelength (μm)
Nadir	
1	0.52–0.60 (green)
2	0.63–0.69 (red)
3N	0.78–0.86 (NIR)
Aft	
3B	0.78–0.86 (NIR)

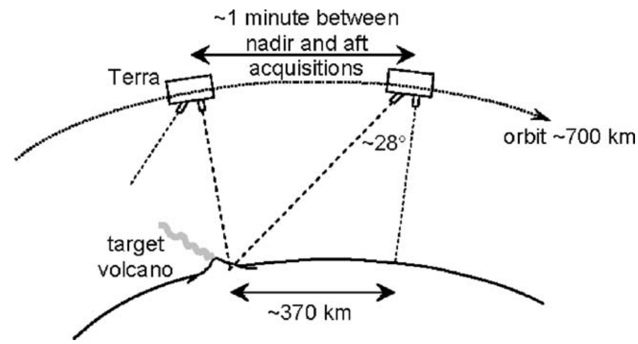

Fig. 2. Schematic diagram of Terra and the ASTER NVIR stereo imaging capability. The target is imaged initially by the nadir sensor, and then again by the aft sensor ∼ 1 min later, creating the stereo effect from which topography can be measured.

4. ASTER topographic mapping methodology

A relatively cloud-free ASTER acquisition of Taranaki was obtained on November 25th, 2000 (Fig. 3a), coinciding with Southern Hemisphere summer when snow cover on the mountain is at a minimum, and relatively cloud-free data of Ruapehu were obtained on January 12th 2001.

For each scene, the nadir and aft images were first compared manually to determine the relative offset between each pixel corresponding to the same position on the surface of the Earth. The offset in the images is almost fully manifest in the along-track direction, and there is a wide range of offsets within a single ASTER acquisition. In practice, for example, if there is a variation in elevation of 2000 m across the scene, an ocean coastline (altitude 0 m a.s.l.) pixel would exhibit zero along-track offset between the aft and nadir images, whereas a 2000 m peak would be offset by ∼ 80 scan lines.

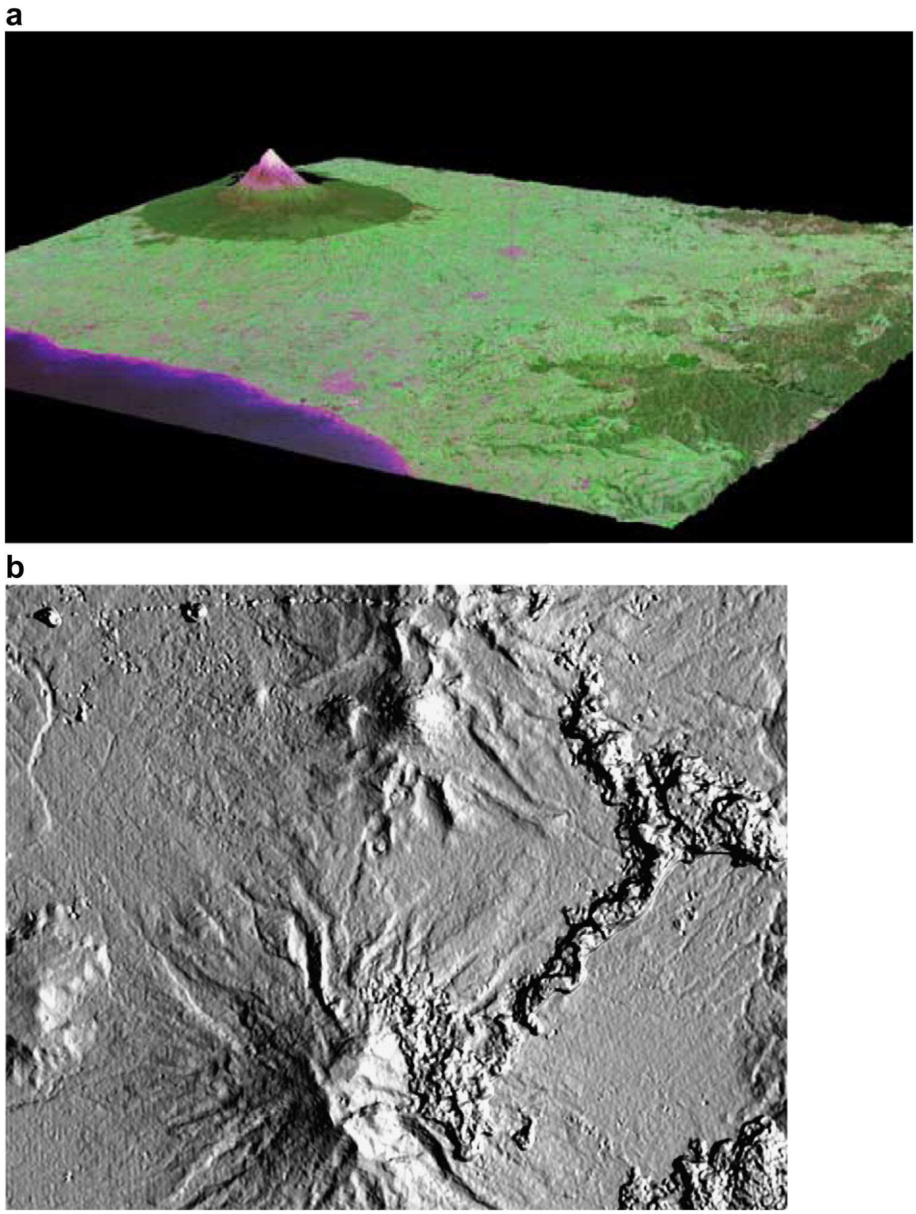

Fig. 3. (a) False color composite derived from bands 1, 2 and 3N of the ASTER nadir image of south eastern Taranaki, draped over the DEM derived from the ASTER stereo pair. (b) Shaded relief image of ASTER DEM of Ruapehu.

We take an iterative, four-step approach for our matching method. We first calculate a rough offset between the nadir and aft views (bands 3N and 3B) for each pixel, and then refine and fine-tune the offset. This is achieved by selecting tie-points common in both images, generating a polynomial (usually of degree 1) to relate nadir coordinates to aft coordinates, and resample the aft scene in nadir space based on this polynomial. A frequency domain cross-correlation is then used to estimate the offset between images at each pixel using a roving kernel, or window of pixels, starting with a kernel of 16×16 pixels. The cross-correlation (Corr) of a kernel in the nadir (n) and the aft (a) is given by the relation:

$$\mathrm{Corr}(n,a) = \mathrm{IFFT}(NA^*), \qquad (1)$$

where N and A are the two-dimensional Fourier transforms of n and a, * represents the complex conjugate of the transform, and IFFT is the inverse Fourier Transform. The maximum value in the resulting Corr(n,a) array is the maximum correlation, and the location within the array provides the offset between aft and nadir images at the kernel location. The kernel size is then decreased successively to 8×16 pixels, 8×8, and 4×8. Each time the kernel size is reduced, the offset is updated by combining the offset and the lag from the new correlation. Inspection of the offset array reveals a significant number of spikes or high frequency noise, which is reduced using a median filter (which preserves correlation peaks). After the 8×8 kernel stage, the final offset is an integer value. In the final

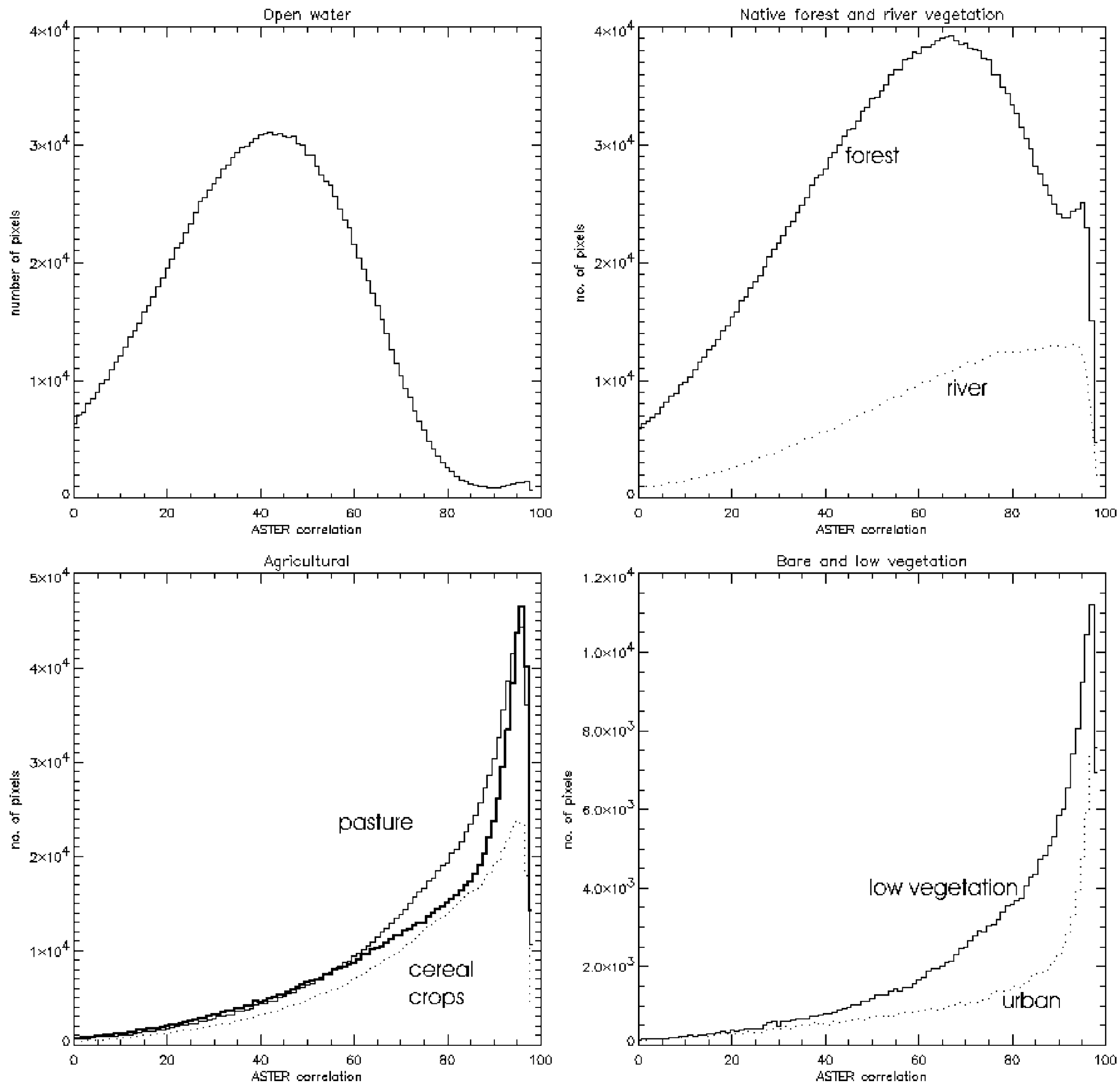

Fig. 4. Histogram plots of estimated pixel correlation for land cover types at Taranaki volcano. Further explanation is provided in the text.

operation, the kernel size is reduced to 4 samples by 8 lines, and a polynomial interpolation on the resulting correlation matrix provides a fractional value for the lag position. This is the final match position.

The relative height (ΔH) of a feature on the landscape is then derived by the relationship:

$$\Delta H = \Delta X/\tan\phi, \quad (2)$$

where ΔX is the parallax, or final match offset, and ϕ is the intersection angle. As the image matching method uses a "kernel" operation, the exact parallax at any point is not calculated, but instead an average parallax for the kernel is derived, and the resulting calculated values of height are essentially smoothed.[1] The resulting ASTER DEMs of Taranaki and Ruapehu (Fig. 3) were georeferenced initially to geographic map coordinates using the supplied ASTER header data, and then refined using known survey trig points identifiable in the false color composite imagery derived from bands 1, 2 and 3N of the nadir image. Comparison of the ASTER DEMs with LINZ digitized data and with surface features in the georeferenced TOPSAR DEMs indicates that the ASTER data are georeferenced to within subpixel accuracy (< 15 m) by this method. The trig points were also used to refine the vertical scaling of the ASTER DEMs interactively, as well as using the assumption that the coastline has zero elevation, in the case of the DEM of Taranaki.

5. ASTER DEM quality assessment

Once georeferenced accurately, the quality of the ASTER DEM data will be affected by a number of factors, including: (1) the presence of cloud in the data, (2) processing

[1] Further queries about the ASTER stereo matching software should be sent to Harold Garbeil, harold@higp.hawaii.edu.

artifacts, (3) the variation in relief across the scene, and, (4) spectral contrast across the kernel used during correlation calculation. Areas covered by cloud are essentially obscured in the visible and near-infrared wavelengths, resulting in gaps in the data. Processing artifacts, such as striping, are mentioned here for completeness as the data in this study are not affected strongly by this problem, but in our experience, some scenes are affected more severely than others. We use a cubic convolution approach, rather than a nearest neighbor algorithm at the initial aft to nadir coarse coregistration stage to reduce striping.

The effects of relief variation and the spectral contrast are not as straightforward to quantify. We note qualitatively here that surface relief is an issue. If a feature in the nadir image looks very different in the aft image due to the effect of parallax, then a good stereo match will be difficult to obtain. Spectral contrast is an issue because in relatively homogeneous regions of spectral reflectance, there are few or no features to match from one scene to the other, as is demonstrated by the correlation distributions in Fig. 4 for land cover types over the ASTER-derived Taranaki DEM. Areas in relief, shadow or with excessively high and low albedo (e.g. snow, salt lakes, some types of forest) may also become problematic during the stereo matching process.

The correlation in Fig. 4 has a different meaning here than in many other image comparisons; in this case, it is a measure of how well the offsets are determined in the ASTER stereo pair. Areas of low correlation are due to temporal decorrelation and to failed cross-correlation determination. Lower relief areas with a reasonable amount of spatial heterogeneity between neighboring pixels should yield the highest correlation. The land cover types were derived from bands 1, 2 and 3N of the nadir image, using standard unsupervised classification techniques (e.g. Lillesand & Kiefer, 1994).

Fig. 4 confirms that open water, an inherently unstable surface, has the lowest correlation statistically. In contrast, agricultural and urban (bare) areas, which have the highest spatial variability, have the highest modal levels of correlation. (It is worth noting that in countries with larger fields than is typical in New Zealand, and hence a lower density of field boundaries, the mean correlation over agricultural land may be much lower.) Indigenous vegetation along rivers has a fairly high overall correlation, whereas native forest is spectrally homogeneous but relatively unchanging between ASTER stereo image acquisitions, and has an intermediate spread of correlation values.

To test the quality of the ASTER DEMs, we looked to Ruapehu volcano (Fig. 1). Unlike Taranaki, other topographic data at a superior accuracy to ASTER DEM data were already available for Ruapehu volcano, because the area was mapped in 1996 and 2000 by airborne interferometric radar, using the NASA TOPSAR system (e.g. Stevens et al., 2002). The TOPSAR DEMs are processed to a 5 m spatial resolution, and have 1–3 m vertical accuracy, depending on the relief (Madsen et al., 1995). This provided an opportunity for the direct comparison between the TOPSAR interferometric DEMs and the ASTER data. We used a TOPSAR swath spanning northern Ruapehu, which was chosen for the variety of slopes and land surface types included in the single swath (Fig. 5). The TOPSAR and ASTER DEMs were georeferenced, and their elevation finetuned using tie-points (in the absence of other, field-measured tie-points) from the LINZ DEM, which is estimated to be accurate to within 10 m vertically, as discussed earlier (Shearer, 1990). Points were chosen with random locations

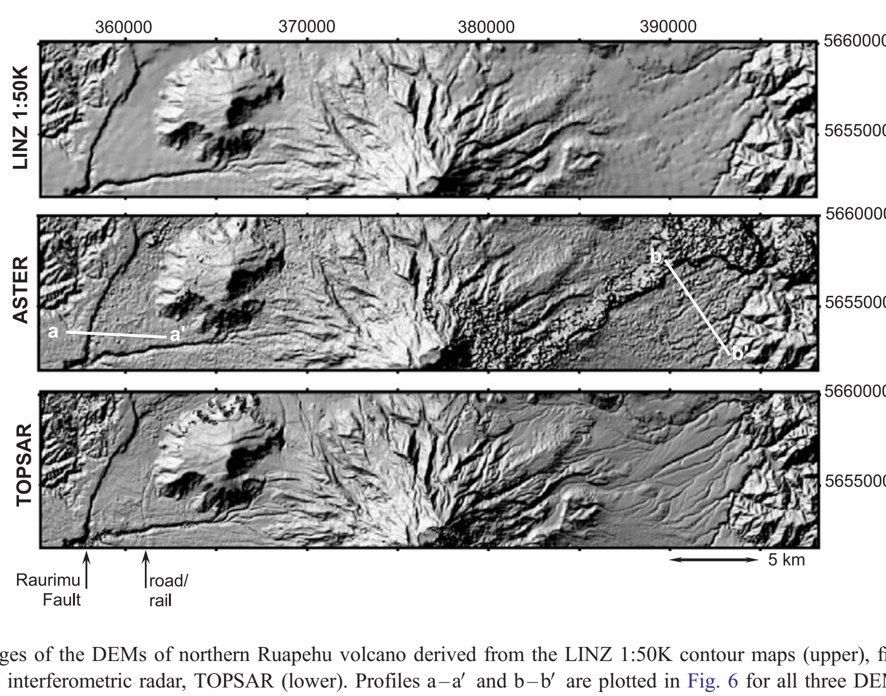

Fig. 5. Shaded relief images of the DEMs of northern Ruapehu volcano derived from the LINZ 1:50K contour maps (upper), from the ASTER stereo pair (centre), and the airborne interferometric radar, TOPSAR (lower). Profiles a–a′ and b–b′ are plotted in Fig. 6 for all three DEMs.

for each swath, (60 points for the ASTER data, 202 points for the TOPSAR data), 2-D polynomial surfaces generated from the tie points, representing the difference between the LINZ and TOPSAR DEMs, and the LINZ and ASTER DEMs. The respective difference surfaces were then subtracted from the respective TOPSAR and ASTER files to produce height-corrected DEMs.

Once height-corrected to the LINZ dataset, the ASTER and TOPSAR DEMs were then subtracted from one another to examine the elevation variability in the ASTER relative to the more accurate TOPSAR data. This is also a measure of the feature preservation. The r.m.s. error of the ASTER DEM relative to the TOPSAR DEM, is then given by:

$$\mathrm{RMSe} = \sqrt{\sum v^2/n}, \quad (3)$$

where v is the height difference, and n is the number of data points, or in this case, pixels (e.g. Shearer, 1990). Excluding differences between the DEMs greater than 100 m, which corresponded to areas covered by cloud in the ASTER data, the histogram of height differences has a normal distribution, centered on zero, indicating that the DEMs are not tilted or displaced significantly relative to one another (Stevens et al., 1999), indicating that the co-warping to the LINZ DEM was identical for both, and that the comparison is valid. Eq. (3) thus gives an overall estimate of RMSe of the ASTER DEM relative to the TOPSAR data of 15.5 m. As the TOPSAR data are estimated to have RMS vertical accuracy of 1–3 m (Madsen et al., 1995), this result is reasonably consistent with published estimates of RMSe for ASTER DEMs (e.g. Hirano et al., 2003; Kääb, 2002; Toutin & Cheng, 2002), and we will come back to this issue in more detail later in this section.

We next examined the preservation of surface features with respect to volcanic flow modeling, because surface roughness and the location and orientation of surface features will to a certain extent govern the speed and direction of flow across a surface, depending on the volume

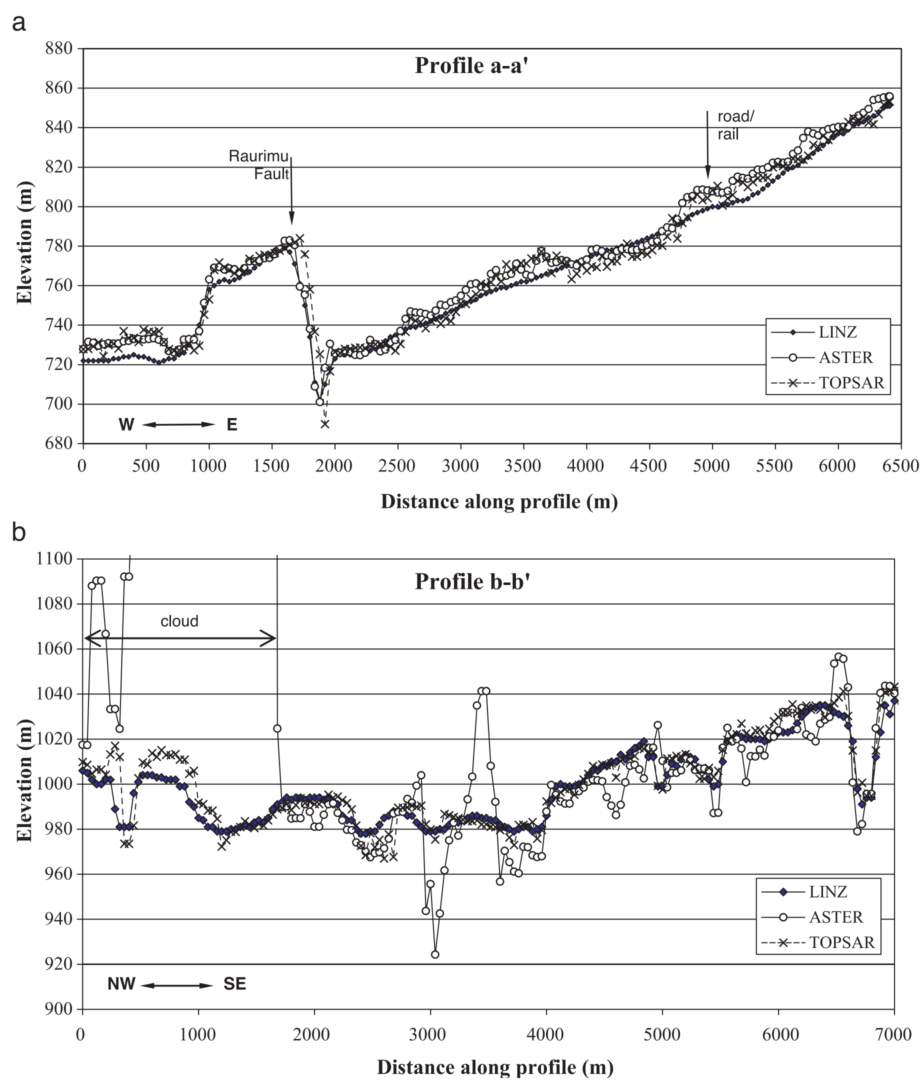

Fig. 6. Profiles of elevation from the DEMs in Fig. 5. (a) Profile a–a′; (b) profile b–b′. For full explanation see text.

and momentum of flowing material (e.g. Loughlin et al., 2002). Conversely, from a modeling point of view, artifacts in a DEM, such as smoothing of features, or inclusion of ''flat spots'' generated during interpolation of sinuous widely spaced contours (Robinson, 1994), will affect the output of volcanic flow simulations (Stevens et al., 2002), so surface feature preservation is important.

The ASTER DEM is an intermediate product between the LINZ and TOPSAR data in terms of feature preservation (Fig. 5). Some of the large stream channels that are not preserved in the LINZ DEM are present in the ASTER DEM. Preservation of the fine-resolution surface detail is examined more closely in profiles a–a′ and b–b′ (Fig. 6). Profile a–a′ shows a strong correlation between undulations in the surface in ASTER and TOPSAR: the Raurimu Fault is represented well by all three DEMs, but smaller features, such as the road and railway surface are preserved in the ASTER and TOPSAR data only.

Conversely, profile b–b′, which was taken across a number of particularly shallow stream channels that are absent in the LINZ DEM (Fig. 5), shows a less consistent match between ASTER and TOPSAR (Fig. 6). The ASTER data in profile b–b′ also seem to have spikes that survive the median filtering. Recalculating the relative RMSe between ASTER and TOPSAR along these profiles gives 6.6 m for profile a–a′, and 19.7 for profile b–b′. It is highly probable that the presence of cloud and atmospheric water vapor on the eastern side of the volcano is detrimental to the ASTER measurements, although the presence of clouds is not evident in bands 1, 2 and 3N. As the RMSe of the TOPSAR DEM is 1–3 m (Madsen et al., 1995), we estimate the absolute RMSe of our Ruapehu ASTER DEM in the absence of cloud noise to be ~ 10 m, which is reasonably consistent with other published estimates (e.g. Hirano et al., 2003; Kääb, 2002; Toutin & Cheng, 2002). The RMSe of other profiles in the vicinity of profile a–a′ is also ~ 10 m. Although the ASTER vertical accuracy is similar to that of the LINZ 1:50 K contour data (Barringer & Lilburne, 1997), the ASTER DEM is a significant improvement in areas between the map contours, where surface features are not preserved during contour interpolation.

6. Discussion

At the time of writing, the ASTER stereo capability is somewhat overshadowed by the impending release of the global Shuttle radar topography mission (SRTM) dataset, and as SRTM covers the most of the Earth's landmass (near complete coverage between latitudes 60° north and south), and is not affected by cloud cover or volcanic plume, one might ask: why bother with ASTER stereo capabilities?

ASTER data have three major advantages over the global SRTM data, which are to be released outside of the US at a 90 m spatial resolution. Firstly, as we have already mentioned, ASTER images include multiple bands spanning the visible to near-infrared range (Table 1), as well as short wave and thermal infrared instruments, which allows land surface cover types to be delineated, as well as fluctuations in volcanic thermal flux to be monitored from night-time images (e.g. Wright et al., 1999). This is not possible with the radars used during the SRTM mission. Secondly, although the ASTER DEM is derived via a kernel method, in the absence of atmospheric contamination, it has a higher resolution and more detailed feature preservation than is possible at a 90 m pixel resolution. Thirdly, the SRTM was a one-off mission, a once-only period of acquisition in February 2000, and there are no plans to fly the instrument again. Since 2000, the SRTM dataset has already become out-of-date at volcanoes where eruptive activity has significantly altered the terrain. For example, in 2000 alone, the topography at the following volcanoes changed significantly enough to outdate the SRTM data: Etna in Sicily, Soputa and Merapi in Indonesia, Usu and Miyake-jima, Japan, Arenal in Costa Rica, Santa Maria in Guatemala, Guagua Pichincha, Altar and Tungurahua in Ecuador, and Copahue, Argentina (Smithsonian Bulletins, 2000). The Terra ASTER instrument is still orbiting, and while SRTM is certainly impressive in terms of global coverage, the ASTER instrument still has an active role in producing up-to-date DEMs at volcanoes provided that the amount of topographic change exceeds the vertical accuracy of the ASTER DEM data (i.e. a few tens of meters or more).

The combined multispectral and stereo capability of the Terra ASTER instrument has a further advantage, apart from the repeatability of measurements. Although the idea of combining multispectral and DEM data at volcanoes is by no means a new one (e.g. Pieri et al., 1990; Wright et al., 2000), ASTER is unique in that the two types of data are provided simultaneously by the same instrument, which speeds up image processing because the data georeferencing, a somewhat time-consuming operation, needs only be attended to once. ASTER data also have the advantage of low cost, public availability, and unlike digitized topographic maps, they have no contour interpolation errors (Robinson, 1994; Stevens et al., 2002). This renders the data ideal for numerous applications, and lastly, we discuss the viability of a few of these here.

Firstly, the ability of perform repeat topographic mapping at volcanoes is important for measuring average rates of mass and volume transport accurately (Stevens et al., 1999), for both additive and subtractive processes, e.g. lava emplacement and sector collapse. However, is the vertical accuracy of ASTER DEMs adequate for this purpose? Certainly, we note that the use of ASTER DEMs will only be helpful for eruptions producing significantly thick deposits, such as superposed lava flow fields (e.g. Stevens et al., 1999), or lava domes (e.g. Watts et al., 2002). On the other hand, although the vertical accuracy of the ASTER DEMs is not sufficient for confident measurement of, for instance, individual basalt lava flows whose thicknesses are of the order of 5–20 m, the aerial extent of thin deposits and surface changes could also easily be detected using the accompanying optical data. Besides, whereas repeat topographic mapping is needed for realistic, accurate measurements in thick and superposed deposits, it is perfectly feasible to estimate the volume of thin deposits to a high accuracy from measurements of areal extent only.

The ASTER data are also especially ideal for strategic volcanic economic risk delineation, and we discuss aspects of this briefly here. With the advent, and increasing use of, computerized volcanic flow models in the last decade (e.g. Ishihara et al., 1990; Schilling, 1998), there has been an increasing demand for accurate, up-to-date DEMs. The SRTM data fill this gap, as prior to this mission, many of the world's volcanoes were mapped poorly, to 1:100,000 or more coarsely, and as long as ASTER is still orbiting and functioning, it provides the means to obtain sufficiently accurate and detailed DEMs for updates that will be needed sporadically at active volcanoes.

The additional advantage of the contemporaneous optical data to complement the DEMs and update the associated changes in land surface cover following eruptions remains to be explored fully. For example, the ASTER combined multispectral and DEM data would allow flow models to be developed that take into account the frictional properties of the surface over which they flow, taken from up-to-date standard land cover classifications from the ASTER bands 1, 2 and 3. There is also the potential to use the combined flow modeling and land surface cover data to examine the risk of secondary hazard from fire spread (Mohammadi et al., 1994; D. Heron, personal communication, 2001) after hot volcanic products are deposited, as well as the seasonal variance of this risk for different land cover types. At Taranaki, the economic risk in terms of damage to agricultural land and local gas and oil refinery and pipeline structures could be rapidly calculated using standard geographical information systems (GIS) techniques, allowing the human and economic impact of a debris avalanche to be estimated, for example, for insurance or local governmental planning purposes. Although we do not pursue it here, a more detailed investigation of the vulnerability of the Taranaki region using ASTER data will be conducted in future (K. Finnis, personal communication, 2003).

The problems we anticipate with ASTER are: (1) obtaining data that are plume-free during an eruption, (2) obtaining cloud-free data in countries with temperate climates, such as New Zealand, and (3) the difficulty of obtaining accurate measurements in areas covered in dense forest—in terms of low albedo, low spatial variability, and of mapping the surface canopy, rather than the forest floor. The temporal resolution of repeat acquisitions is also an issue: this is not adequate to guarantee the imaging of the most rapid transient events during a volcanic eruption, and as such, ASTER data are not optimal for operational use. However, the benefits derived from the availability of ASTER data outweigh the problems, and many useful applications remain viable.

7. Conclusion

We have developed semi-automated software to derive topographic data from ASTER VNIR stereo pairs, and have investigated the quality of the resulting DEMs at two of New Zealand's active volcanoes, in terms of surface feature preservation and vertical accuracy. The potential of ASTER data has been somewhat overshadowed by the impending release of the SRTM dataset. However, the data acquired by the on-going ASTER mission remain highly valuable to the volcanology community, and elsewhere, and their value should not be overlooked.

Acknowledgements

The work was funded by the Foundation for Research in Science and Technology and the Earthquake Commission of New Zealand. The ASTER data were provided by the USGS Eros Center. Thanks to Vernon Manville (GNS) for useful discussion, to internal reviewers David Barrell and David Heron. We thank the three anonymous external referees, whose comments improved the manuscript significantly.

References

Abrams, M. (2000). ASTER: Data products for the high spatial resolution imager on NASA's Terra platform. *International Journal of Remote Sensing*, *21*, 847–853.

Adams, R. D., & Ware, D. E. (1977). Subcrustal earthquakes beneath New Zealand: Locations determined with a laterally inhomogeneous velocity model. *New Zealand Journal of Geology and Geophysics*, *20*, 59–83.

Alloway, B., Neall, V. E., & Vucetich, C. G. (1995). Late quaternary (post 28,000 year BP) tephrostratigraphy of northeast and central Taranaki, New Zealand. *Journal of the Royal Society of New Zealand*, *25*, 385–458.

Barringer, J. R. F., & Lilburne, L. (1997). An evaluation of digital elevation models for upgrading New Zealand land resource inventory slope data. *Proceedings of the Second Annual Conference of GeoComputation 1997, University of Otago, New Zealand, 26–29 August 1997* (pp. 109–116).

Bryan, C. J., & Sherburn, S. (1999). Seismicity associated with the 1995–1996 eruptions of Ruapehu Volcano, New Zealand; narrative and insights into physical processes. *Journal of Volcanology and Geothermal Research*, *90*, 1–18.

Christenson, B. W., & Wood, C. P. (1993). Evolution of a vent-hosted hydrothermal system beneath Ruapehu Crater Lake, New Zealand. *Bulletin of Volcanology*, *55*, 547–565.

Hackett, W. R., & Houghton, B. F. (1989). A facies model for a Quaternary andesitic composite volcano, Ruapehu, New Zealand. *Bulletin of Volcanology*, *51*, 51–68.

Hirano, A., Welch, R., & Lang, H. (2003). Mapping from ASTER stereo image data: DEM validation and accuracy assessment. *Photogrammetry and Remote Sensing*, *57*, 356–370.

Ishihara, K., Iguchi, M., & Kamo, K. (1990). Numerical simulation of lava flows on some volcanoes in Japan. In J. H. Fink (Ed.), *Lava flows and domes. IAVCEI proceedings in volcanology*, *vol. 2* (pp. 174–207). Heidelberg: Springer-Verlag Press.

Johnston, D. M., Houghton, B. F., Neall, V. E., Ronan, K. R., & Paton, D. (2000). Impacts of the 1945 and 1995–1996 Ruapehu eruptions, New

Zealand: An example of increasing societal vulnerability. *Geological Society of American Bulletin*, *112* (5), 720–726.

Kääb, A. (2002). Monitoring high-mountain terrain deformation from repeated air- and spaceborne optical data: Examples using digital aerial imagery and ASTER data. *ISPRS Journal of Photogrammetry and Remote Sensing*, *57*, 39–52.

Land Information New Zealand (1987). 1:50,000 Topographic map, Kakatahi, Edition 1 1987, 260-S21.

Land Information New Zealand (1996). 1:50,000 Topographic map, Ohakune, Edition 2 1996, 260-S20.

Land Information New Zealand (1996). 1:50,000 Topographic map, Tongariro, Edition 2 1994, Limited revision 1996, 260-T19.

Land Information New Zealand (1997). 1:50,000 Topographic map, Ruapehu, Edition 2 1994 Limited revision 1997, 260-T20.

Land Information New Zealand (1998). 1:50,000 Topographic map, Taihape, Edition 1 1982 Limited revision 1998, 260-T21.

Land Information New Zealand (1999). 1:50,000 Topographic map, Taranaki, Edition 1 1999, 260-P20.

Land Information New Zealand (2000). NZ Topo Data Dictionary—documentation guide version 2.2. Unpublished.

Lillesand, T. M., & Kiefer, R. W. (1994). *Remote sensing and image interpretation*. New York: Wiley (750 pp.).

Loughlin, S. C., Calder, E. S., Clarke, A., Cole, P. D., Luckett, R., Mangan, M. T., Pyle, D. M., Sparks, R. S. J., Voight, B., & Watts, R. B. (2002). Pyroclastic flows and surges generated by the 25 June 1997 dome collapse, Soufriere Hills Volcano, Montserrat. In T. H. Druitt, & B. P. Kokelaar (Eds.), *The eruption of the Soufriere Hills volcano, Montserrat, from 1995 to 1999. Memoirs*, *vol. 21* (pp. 191–209). London: Geological Society.

Madsen, S. N., Martin, J. M., & Zebker, H. A. (1995). Analysis and evaluation of the NASA/JPL TOPSAR across-track interferometric SAR system. *I.E.E.E. Transactions on Geoscience and Remote Sensing*, *33*, 383–391.

Mohammadi, J., Alyasin, S., & Bak, D. N. (1994). Risk analysis of post-earthquake fires. In J. Mohammadi, S. L. McCabe, & R. Villaverde (Eds.), *Proceedings of the U.S. National Conference on Earthquake Engineering, 5*, *vol. 4* (pp. 679–688).

Neall, V. E., & Alloway, B. V. (1993). Volcanic hazards at Egmont volcano. (2nd ed.) *Ministry of Civil Defence volcanic hazards information series*, *1*, (32 pp.).

Neall, V. E., Stewart, R. B., & Smith, I. E. M. (1986). History and petrology of the Taranaki volcanoes. In I. E. M. Smith (Ed.), *Late cenozoic volcanism in New Zealand* (pp. 251–263). Royal Society of New Zealand Bulletin.

Palmer, B. A., Alloway, B. V., & Neall, V. E. (1991). Volcanic-debris-avalanche deposits in New Zealand—lithofacies organization in unconfined, wet-avalanche flows. *Society of Economic Paleontologists and Mineralogists Special Publication*, *45*, 89–98.

Palmer, B. A., & Neall, V. E. (1989). The Murimotu Formation: 9500 year old deposits of a debris avalanche and associated lahars, Mount Ruapehu, North Island, New Zealand. *New Zealand Journal of Geology and Geophysics*, *32*, 477–486.

Palmer, B. A., & Neall, V. E. (1991). Contrasting lithofacies architecture in ring-plain deposits related to edifice construction and destruction, the Quaternary Stratford and Opunake Formations, Egmont Volcano, New Zealand. *Sedimentary Geology*, *74*, 71–88.

Pieri, D. C., Glaze, L. S., & Abrams, M. J. (1990). Thermal radiance observations of an active lava flow during the June 1984 eruption of Mount Etna. *Geology*, *18*, 1018–1022.

Robinson, G. J. (1994). The accuracy of digital elevation models derived from digitised contour data. *Photogrammetric Record*, *14*, 805–814.

Schilling, S. P. (1998). LAHARZ: GIS programs for automated mapping of lahar-inundation hazard zones. US Geological Survey Open-File Report 98-638, 79 pp.

Shearer, J. W. (1990). The accuracy of digital terrain models. In G. Petrie, & T. J. M. Kennie (Eds.), *Terrain modelling in surveying and civil engineering* (pp. 315–336). London: WPS.

Smithsonian Bulletins (2000, March 2000–December 2000). *Bulletin of the global volcanism network* (Washington, USA).

Stevens, N. F., Manville, V., & Heron, D. W. (2002). The sensitivity of a volcanic flow model to digital elevation model accuray: experiments with digitized map contours and interferometric SAR at Ruapehu and Taranaki volcanoes, New Zealand. *Journal of Volcanology and Geothermal Research*, *199*, 89–105.

Stevens, N. F., Wadge, G., & Murray, J. B. (1999). Lava flow volume and morphology from digitised contour maps: A case study at Mount Etna, Sicily. *Geomorphology*, *28*, 251–261.

Toutin, T., & Cheng, P. (2002). Comparison of automated digital elevation model extraction results using along-track ASTER and across-track SPOT stereo images. *Optical Engineering*, *41*, 2102–2106.

Wadge, G., Scheuchl, B., & Stevens, N. F. (2002). Spaceborne radar measurements of the eruption of Soufriere Hills Volcano, Montserrat. In T. H. Druitt, & B. P. Kokelaar (Eds.), *The eruption of the Soufriere Hills Volcano, Montserrat, from 1995–1999. Memoirs*, *vol. 21* (pp. 583–594). London: Geological Society.

Watts, R. B., Herd, R. A., Sparks, R. S. J., & Young, S. R. (2002). Growth patterns and emplacement of the andesite lava dome at Soufriere Hills Volcano, Montserrat. In T. H. Druitt, & B. P. Kokelaar (Eds.), *The eruption of the Soufriere Hills Volcano, Montserrat, from 1995–1999. Memoirs*, *vol. 21* (pp. 115–152). London: Geological Society.

Welch, R., Jordan, T., Lang, H., & Murakami, H. (1998). ASTER as a source for topographic data in the late 1990's. *I.E.E.E. Transactions on Geoscience and Remote Sensing*, *36*, 1282–1289.

Werner, M. (2001). Shuttle Radar Topography Mission (SRTM) mission overview. *Frequenz*, *55*, 75–79.

Wright, R., Rothery, D. A., Blake, S., & Harris, A. J. L. (1999). Simulating the response of the EOS Terra ASTER sensor to high-temperature volcanic targets. *Geophysical Research Letters*, *26*, 1773–1776.

Wright, R., Rothery, D. A., Blake, S., & Pieri, D. C. (2000). Visualising active volcanism with high spatial resolution satellite data: The 1991–1993 eruption of Etna. *Bulletin of Volcanology*, *62*, 256–265.

Zebker, H. A., Werner, C. L., Rosen, P. A., & Hensley, S. (1994). Accuracy of topographic maps derived from ERS-1 interferometric radar. *I.E.E.E. Transactions on Geoscience and Remote Sensing*, *32*, 823–883.

Zomer, R., Ustin, S., & Ives, J. (2002). Using satellite remote sensing for DEM extraction in complex mountainous terrain: Landscape analysis of the Makulu Barun National Park of eastern Napal. *International Journal of Remote Sensing*, *23*, 125–143.